Classification of Deflections of Thin-Walled Elements Made of EN AW-7075A Aluminum Alloy During Milling

Jakub Czyżycki[1*], Lidia Marciniak-Podsadna[2], Paweł Twardowski[1]

[1] Division of Machining, Institute of Mechanical Technology, Faculty of Mechanical Engineering, Poznan University of Technology, ul. Piotrowo 3, 60-965 Poznan, Poland

[2] Division of Metrology and Measurement Systems, Institute of Mechanical Technology, Faculty of Mechanical Engineering, Poznan University of Technology, ul. Piotrowo 3, 60-965 Poznan, Poland

* Corresponding author's e-mail: jakub.czyzycki@put.poznan.pl

ABSTRACT

The aim of the research is to classify and evaluate the size of deformations appearing during milling of thin-walled elements representing a pocket form made of aluminum alloy EN AW-7075A. Finishing, which is the purpose of the research, was carried out at the full depth of cut a_p = 15 mm, milling the entire height of the wall in one pass. Deformations during machining were correlated with the geometric accuracy of the workpieces after machining. During the tests, deformations were measured with a laser displacement sensor, and the temperature of the samples was measured using a resistance temperature sensor. The tests made it possible to identify deformations occurring during the milling of thin-walled elements. The course of deformation during milling was analyzed, from which the value of deformation caused by milling, the reaction to this deformation and its time were extracted, additionally, permanent distortion of the workpiece was detected. The results show the effect of the ratio of the height to the thickness of the thin-walled element on its geometric accuracy after machining in the form of straightness and flatness of the samples. The test results were compared to the tests carried out on the Ti6Al4V titanium alloy, which confirmed the influence of the material selection on the course of deformations during milling.

Keywords: thin-walled elements milling, workpiece deformation, aluminum alloy milling.

INTRODUCTION

As discussed in studies [1, 2], in order to reduce weight in the aviation industry and increase capacity, the number of thin-walled monolithic elements that are produced by milling is increasing. Machining of such elements requires an individual approach due to the low stiffness of the workpiece, the risk of vibrations and deformations, which causes manufacturing errors [3]. The benefits of using monolithic structures containing thin-walled elements are associated with the aforementioned difficulties during machining, which are solved in a number of ways. The authors divide the methods of elimination vibrations into passive and active [1, 4]. The elimination of vibrations during the machining of thin-walled

elements is an important aspect and widely discussed by many authors [5, 6], while it is also important to understand the deformation process itself - that is, what happens to the thin-walled element during and after machining. Other methods that allow to improve the quality and accuracy of thin-walled elements are the selection of an appropriate machining method. The research [7] presents a comparison of high-performance machining methods with traditional ones in favor of HSC (high speed cutting). In addition to the selection of technological parameters, the strategy for machining thin-walled elements is important. As presented in the studies of Kuczmaszewski et al. [8], multi-row milling of thin walls and variants of this method achieves better results than milling at the full depth of the wall.

In order to avoid vibrations, it can be use the determination of stability lobes, which have been used for many years in the selection of optimal parameters to ensure stable processing. Many researchers present new ways to determine them [9, 10]. The authors of [9] were able to predict global (overall) stability for a compliant workpiece during milling using time-domain simulations. A different approach was presented in the study [10], authors took into account the volume of material removed to predict the stability of thin-walled elements during milling. A new computational model was presented that separates the workpiece into solid particles and particles removed using the Ritz method, the results were confirmed experimentally.

As presented in the studies of Soori and Asmael [11] and in Figure 1, the dimensional error of the milled surface is the sum of deformations caused by the components of the cutting force and thermal deformations. Where $\delta_{t,p}$ and $\delta_{f,p}$ are the normal projections of the cutting force and the deflection error induced by the cutting temperature for point P, respectively. In addition, R_N and R_A are the nominal and specified radial depth of cut, respectively.

Many studies, including own studies [12, 13], were carried out on straight-form walls in which the geometry focused only on the difference in their thickness and height. Such selection of thin-walled elements for research purposes simplifies their analysis and modelling. The actual shapes of thin-walled elements are pocket structures with thin bottoms and walls, and complex shapes [14, 15]. The influence of the geometric shape of the workpiece with thin-walled elements on the accuracy after machining was confirmed by research [16]. Appropriate selection of shape and ribs can reduce post-machining deformations. When using the conclusions of such studies in real conditions, this aspect should be taken into account.

Residual stresses in machining are a topic widely discussed in the literature, in the subject of machining thin-walled elements they are often crucial when it comes to their impact on the accuracy after machining. These stresses cause significant errors in the manufacture of thin-walled objects, as presented in [17]. In addition, the positive effect of machining a thin-walled element on both sides (e.g. rotor blades) on the distribution of stresses has been proven, provided that the stresses caused by the next pass are lower than during the first pass. As a result, there is no need to use stress relieving annealing. Having access to newer and newer computational technologies, such as the FEM environment, the authors use those to predict the aforementioned deformations caused by the stresses of thin-walled elements caused by machining. The authors [18], using the AdvantEdge™ software, tested several thin-walled component machining strategies, receiving information on the components of the cutting force, process temperature and stresses generated during machining. Each of the four strategies leaves a different stress distribution. The simulation carried out allowed for the selection of a strategy that was experimentally verified with a satisfactory effect. The subject of residual stresses during the machining of thin-walled elements is discussed in various forms. The author [19] showed that a endmill with a diameter of 16 mm reduced residual stresses by up to 35% in relation to a endmill with a diameter of 8 mm, going further - using a endmill with a diameter of 12 mm, the authors reduced deformations after machining by 60%. Studies [18] and others [20, 21]
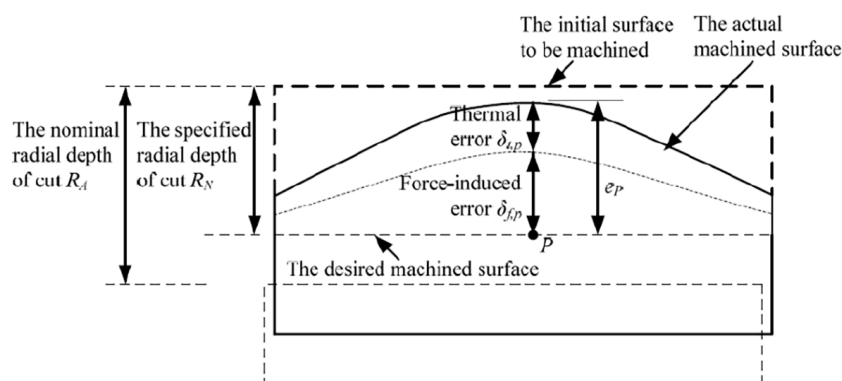

Fig. 1. Manufacturing error caused by deformations from the milling process and thermal deformations [11]

show the effectiveness in models used to predict post-machining deformations, which saves time and money, which are so important in industries where such shapes of elements occur.

In the presented studies, the subject of the influence of material selection on a thin-walled element was discussed, it was analyzed in terms of the course of deformations during milling. As research [16] shows, a thin-walled element made of EN AW-6082 with better plasticity and machinability than EN AW-7075 showed a lower total deformation after machining. A similar comparison was made in research [22] where aluminum alloys EN AW-2024 and EN AW-7075 were milled with different technological parameters, comparing residual stresses after machining. The result of the research is the selection of optimal machining parameters ensuring minimum stresses.

The aim of the research was to classify deformations and their size during milling of a thin-walled element made of aluminum alloy EN AW-7075. The results were correlated with the geometrical accuracy after machining, which is an indicator of the correct performance of the workpiece. The shape and material selection in the processing of thin-walled elements were analyzed. An additional objective of the research is to determine the feasibility of measuring the temperature of a thin-walled component during machining.

MATERIALS AND METHODS

Milling of thin-walled elements made of EN AW-7075A alloy was carried out on a three-axis milling center DECKEL MAHO model DMC 70V. Solid carbide endmills were used for machining, endmill with a diameter of $d = 8$ mm, a number of teeth $z = 2$, the helix angle $\lambda_s = 40°$ and the rake angle $\gamma = 20°$ (FRAISA C15620391, figure 2) was used for roughing, while a endmill with a diameter of $d = 8$ mm was used for finishing, the number of teeth $z = 6$, the helix angle $\lambda_s = 40°$ and the rake angle $\gamma = 20°$ (FRAISA C15589391, figure 3). Both tools had the Celero coating which Fraisa uses on its aluminum tools to increase durability.

The tools were mounted through KELCH thermal holders. The machining was carried out without any coolant. The workpiece is shown in figure 4, it has a cuboid-shaped base that was used to attach to the measurement platform and a thin-walled element representing a pocket form. The tests were carried out on 6 variants of the samples, each of them differing in wall thickness, the variants of the samples are presented in Table 1. Firzgerald proposed the classification of thin-walled elements as an object whose height-to-thickness ratio exceeds 10:1, in the research presented, the samples are in the range of 7.5–30 h/t [23]. By using the height-to-thickness (h/t) ratio reference of a thin-walled component instead of thickness alone, it is more clearly to compare and use the methods and test results in further experiments. Such a scheme can be seen in many articles on machining thin-walled components [24, 25]. P and the number after it is the height-to-thickness ratio, while S1-4 indicates the sample number. In addition to determining only the thickness of the thin-walled element, the parameter which is the ratio of the height h to the wall thickness t was used in the tests. The technological parameters are shown in Table 2 below. The purpose of roughing machining was to give the assumed shape designed in Autocad Inventor with a thickness allowance of 0.2 mm with parameters and a strategy that allowed for the smallest possible deformation after roughing machining. During the tests, this allowance was milled in two passes at the full depth of cut ($a_p = 15$ mm) and the milling width $a_e = 0.1$ mm. The samples were climb milled.

Semi-finished products in the form of rectangular cubes were mounted each time on a designed measurement platform (Figure 5) which ensured the possibility of roughing and finishing in one mounting. In addition, during finishing milling, a Micro-Epsilon optoNCDT ILD1700-10 LL laser displacement sensor was used, which was attached to the platform. The displacement laser sensor was aimed at the inside of the wall in the middle of its length and at a distance of 1.5 mm from the top of the wall. The temperature measurement of the thin-walled element was carried

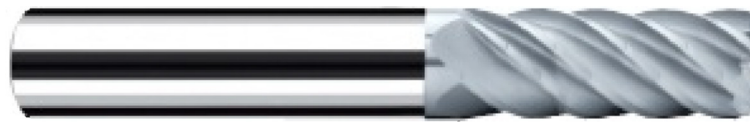**Fig. 2.** Roughing endmill with a diameter of $d = 8$ mm (FRAISA C15620391)

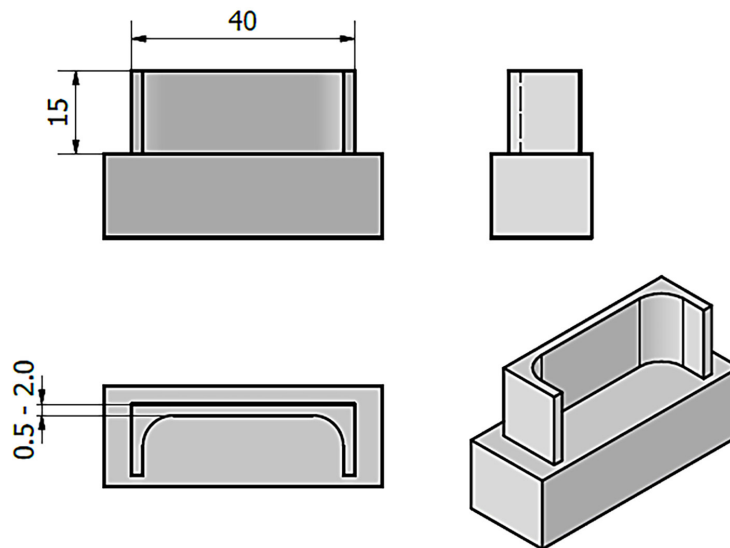**Fig. 3.** Finishing endmill with a diameter of *d* = 8 mm (FRAISA C15589391)

Fig. 4. Tested thin-walled element

Table 1. Variants of the tested samples (EN AW-7075A)

Sample	*h/t* ratio	Thickness after machining [mm]
P1S1 – P1S4	7.5	2.00
P2S1 – P2S3	10	1.50
P3S1 – P3S4	12	1.25
P4S1 – P4S3	15	1.00
P5S1 – P5S4	20	0.75
P6S1 – P6S3	30	0.50

Table 2. Technological parameters (EN AW-7075A)

Parameter	Rough	Finishing
Cutting speed v_c [m/min]	250	450
Cutting feedrate v_f [mm/min]	1000	5000
Cutting depth a_p [mm]	2	15
Cutting width a_e [mm]	2	0.1

out using a PT100 resistance temperature sensor glued with AG TermoGlue thermal conductive adhesive as shown in Figure 6. The reading was carried out using a universal temperature meter by Apar. Due to the limited speed of signal recording with the temperature sensor, temperature measurements are presented only on two samples (sample 1 and 2) in the range of h/t 7.5–20.

The measurement of the geometrical accuracy of the thin-walled elements was carried out on the DEA Global Image 775 coordinate measuring machine with the limiting error MPEE = 1.5+L/333. The SP25m RENISHAW head with a 40 mm long pin and a ruby ball with a diameter of 6 mm was used for the measurements. During the tests, straightness and flatness at 10 heights
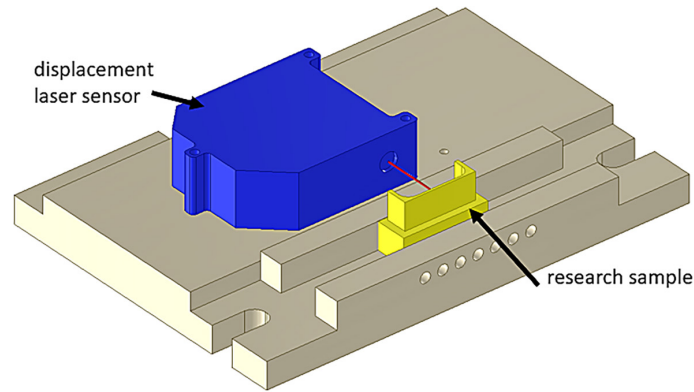
Fig. 5. Measurement platform

Fig. 6. Location of the resistance temperature sensor on the sample

were determined in accordance with figure 7, and the thickness of the samples in their central part, as shown in Figure 8. In addition, for comparative purposes and the possibility of a broader analysis of deformation during milling and the description of thermal phenomena occurring during milling of thin-walled parts, the results of similar studies on titanium alloy Ti-6Al-4V (grade 5) are presented in the discussion section. The tests were realized on samples with a pocket form wall as in Figure number 4. The tests of deformation were also carried out in the range of h/t ratio equal to 7.5–30. The cutting conditions are shown in Table 3. A set of two solid carbide uncoated milling endmills with diameters of $d = 10$ mm was used for machining. Roughing machining was carried out with a cutter (FRAISA P8800.450) with a number of teeth $z = 4$, the helix angle $\lambda_s = 40°$ and the rake angle $\gamma=5°$. Finishing machining was done with a cutter (FRAISA P8401.450) with a number of teeth $z = 7$, the helix angle $\lambda_s = 55°$ and the rake angle $\gamma = 10°$. The machining was carried out without any coolant.

RESULTS

According to the description of the milling strategy, in the case of finishing, it was carried out over the full height of the wall with the milling width $a_e = 0.1$ mm in two passes one after the other. Figure 9 shows an exemplary course of deformation of a thin-walled element (sample P6S1) measured with the use of a laser displacement sensor. In addition, a model of the sample was plotted on the plot along with its coordinate system in order to more easily understand the direction of deformations occurring during milling.

The deformation course can be divided into several sections, as shown in Figure 10 on the example of the first pass. The ABC section is the reaction of the thin wall to the milling process, the deformation value (section AB measured in the Y axis) is 56 μm, this deformation is to the inside of the thin-walled element. The CDE section is the reaction of the wall to the previous deformation, the value of this reaction is 17.6 μm (CD section measured in the Y axis) and the opposite
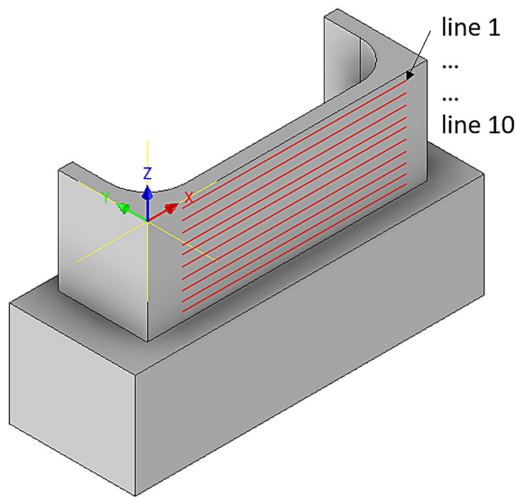
line 1
...
...
line 10

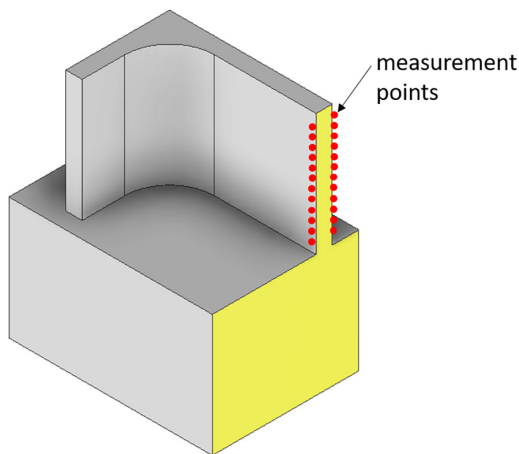**Fig. 7.** Place for determining the straightness on the sample

measurement points

Fig. 8. Thickness measurement location on the sample

direction, i.e. outside the wall. An important aspect is the time in which the thin-walled element returns to the stable state – section DE, the return time is 3.6 s. In addition to returning to a stable state, it should be noted that there is a difference between the position of the wall before milling and after milling, which means that permanent distortion of the workpiece occur. The value of this distortion after the first pass in this case is 7.1 μm (section AE measured in the Y axis). The

same situation occurs during the second pass. The deformation value is greater due to the lower wall thickness after the first pass. The value of the described deformations is in the Y-direction. The size of the described deformation is in the range of 1–7 μm in the tested samples, but at the moment there is not a correlation with, for example, the h/t ratio, additionally, several samples of the same thickness have large differences between the mentioned permanent distortions. A more detailed analysis of the discussed deformations can be found in point 4 of the tests.

The results of temperature measurement during the processing of the samples are shown in Figure 11. An increase in temperature can be seen with an increase in the h/t ratio, i.e. with a decrease in the thickness of the sample – this is due to the closer and closer distance of the temperature sensor from the cutting zone and better temperature conductivity to the measuring area. It can be assumed that for the tested samples the temperature of the sample increases to 60–105 °C. Temperature measurement in machining is a difficult phenomenon, and in the subject of machining thin-walled parts it is unheard of in the literature. The essence of the measurements presented here was to determine the feasibility of their measurement for potential use in simulation studies of thermal deformation.

The results of the thickness of the samples are shown below, an example of a CMM measurement report is shown in Figure 12. The difference between the wall thickness at the bottom and the nominal value was determined by the parameter Δb (bottom) and the parameter Δt (top). The results of the parameters Δb and Δt as a function of the h/t ratio are shown in Figure 13. In this graph, a characteristic problem can be noticed when machining thin-walled elements, which consists in deforming the upper part of the wall and creating a "triangular" shape expanding upwards. The parameter Δb does not exceed 0.15 mm, with more than 0.30 mm for the parameter Δt. The course of deformations shown in Figures 9–10 is the reason

Table 3. Technological parameters (Ti-6Al-4V)

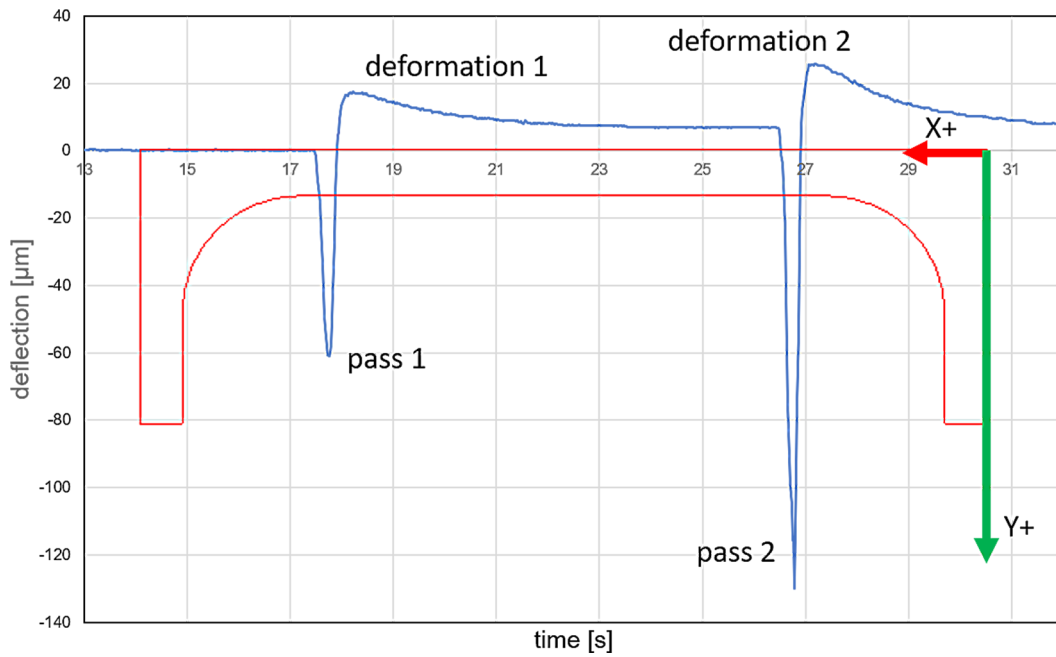| Parameter	Rough	Finishing
Cutting speed v_c [m/min]	45	60
Cutting feedrate v_f [mm/min]	150	400
Cutting depth a_p [mm]	4	15
Cutting width a_e [mm]	1	0.1

Fig. 9. An exemplary deformation diagram with a sample model marked on it P6S1 ($h/t = 30$)
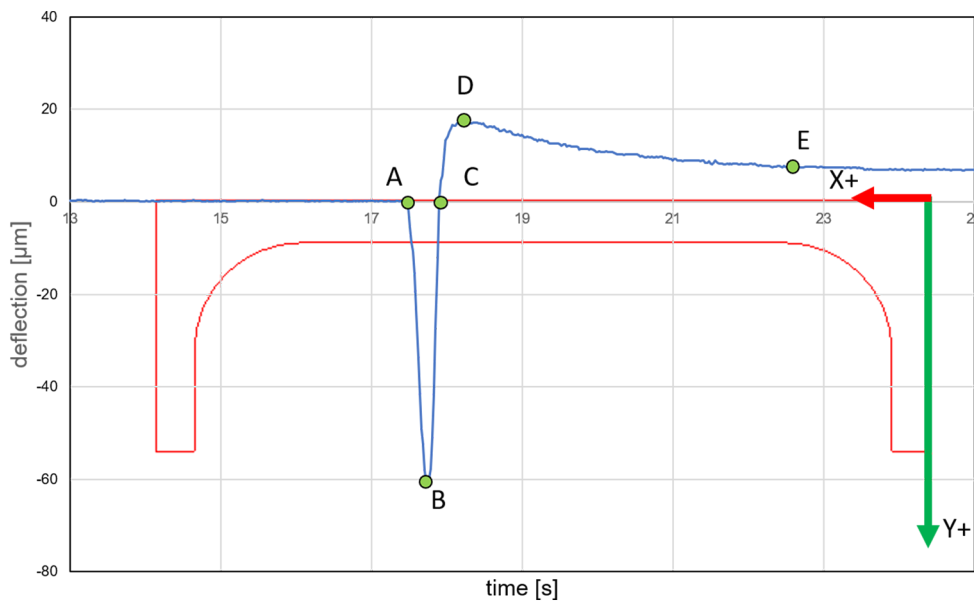

Fig. 10. The example course of the deformation of the thin-walled element
during the first pass of the endmill P6S1 ($h/t = 30$)

for the deflection of the thin-walled element visible in the straightness and flatness measurement results. Figure 14 shows an exemplary straightness result of one of the measurement lines of the P6S2 sample. As before, the model of the sample along with the coordinate system was superimposed on the result. The visible arrows show the deviation from the mean square line. Figure 15 shows the result from the flatness measurement report of the same sample.In addition to the test samples, samples with the designation "blank" were distinguished in the tests, these are samples on which only roughing was performed and have an allowance for finishing. The straightness of the test samples as well as those marked "blank" is presented in the following graphs (Figure 16). Example blank sample designation: 1.45BL1 means a blank sample with a wall thickness of 1.45 mm on which only rough machining has been carried out, and it is sample number 1 among several
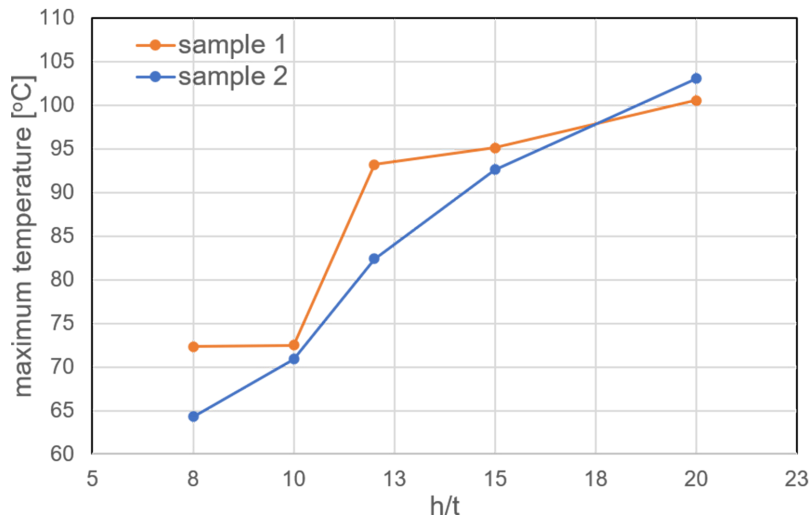
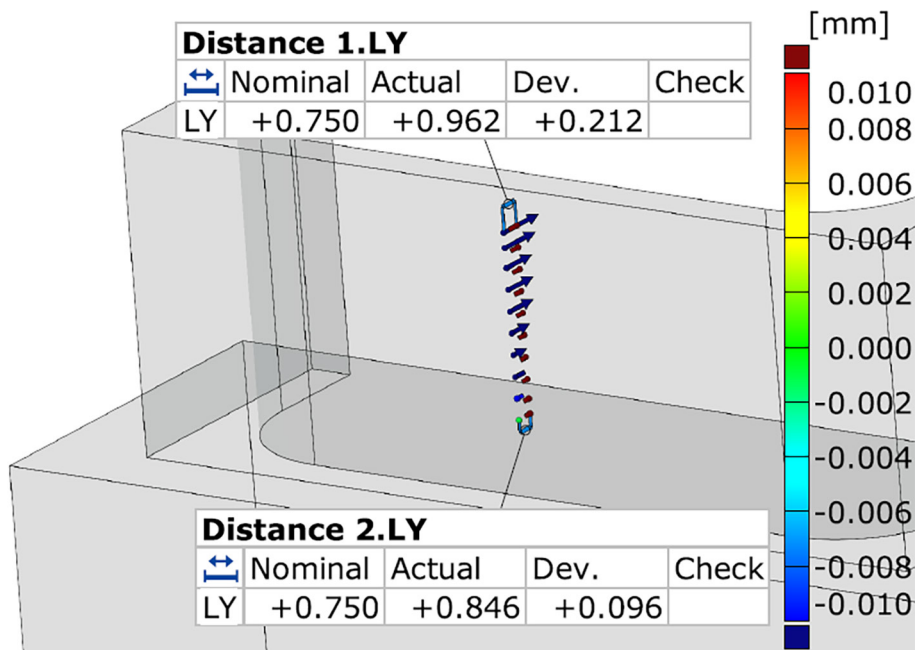**Fig. 11.** Temperature measurement results during milling

Fig. 12. Example CMM report of thickness measurement of the sample P5S1 ($h/t = 20$)

identified samples. The graph show a positive effect of the selection of the milling strategy for roughing, where there is no significant change in straightness along with the measurement number.

The results are in the range of 0.005–0.025 mm. Straight 1 was at the top of the wall. In the case of finished samples, the relationship is different, with the increase of the h/t ratio, a sudden increase in straightness is noticeable the closer to the top of the wall. The P1-P3 samples (samples with a h/t ratio range of 7.5–12) obtained straightness values similar to the "blank" samples, while above the coefficient $h/t = 15$, the straightness

in the samples is high, especially at the top of the sample, exceeding 0.12 mm. The following graphs show the correlation of deformations of a thin-walled element during milling with the geometrical accuracy after machining – flatness. The maximum deformation measured during the second pass machining is taken into account for comparison.

As shown in Figure 17, the effect of deformation during milling on the flatness after machining has a linear relationship. On the other hand, Figure 18 shows the influence of the h/t ratio on flatness. It can be noticed that from the parameter
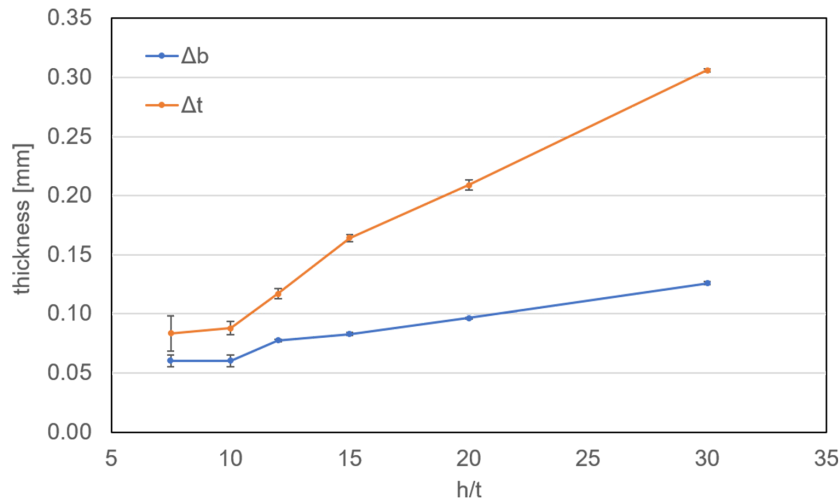
Fig. 13. Parameter values *Δb* (thickness difference at the bottom) and *Δt* (thickness difference at the top)
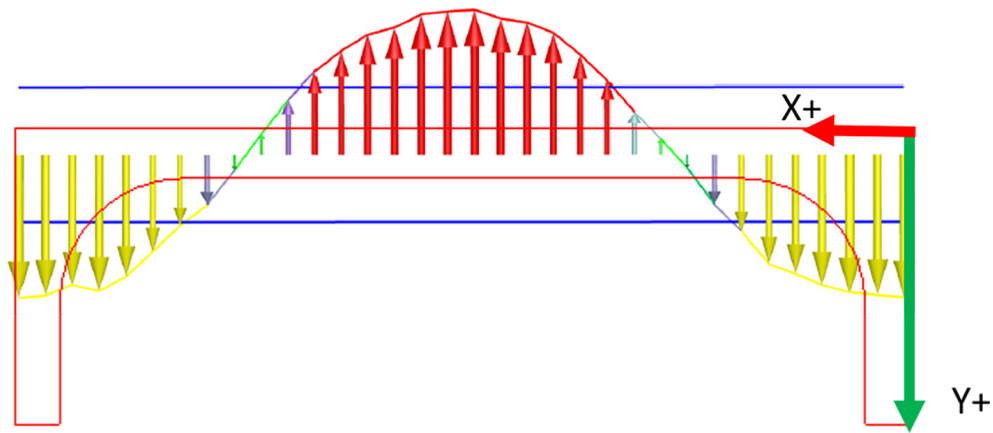

Fig. 14. The straightness of one of the sample measurement lines P6S2 ($h/t = 30$)
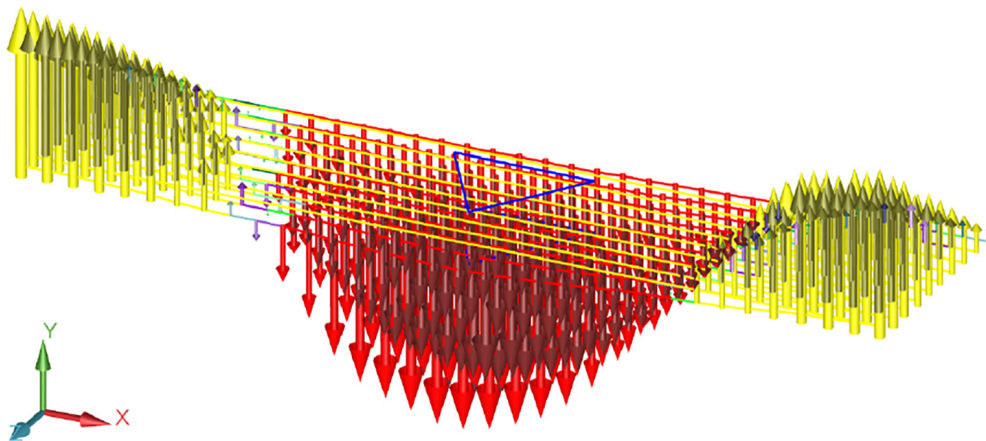

Fig. 15. Flatness of the sample P6S2 ($h/t = 30$)

h/*t* equal to 15 the rate of surface quality deterioration increases, which is confirmed by figure 16. The flatness value for the P1-P3 samples does not exceed 0.030 mm, and finally the flatness of the P6 sample (h/t = 30) is 0.130 mm.

DISCUSSION

The presented tests show how significant the influence on the accuracy of thin-walled elements is their thickness, and more specifically the ratio
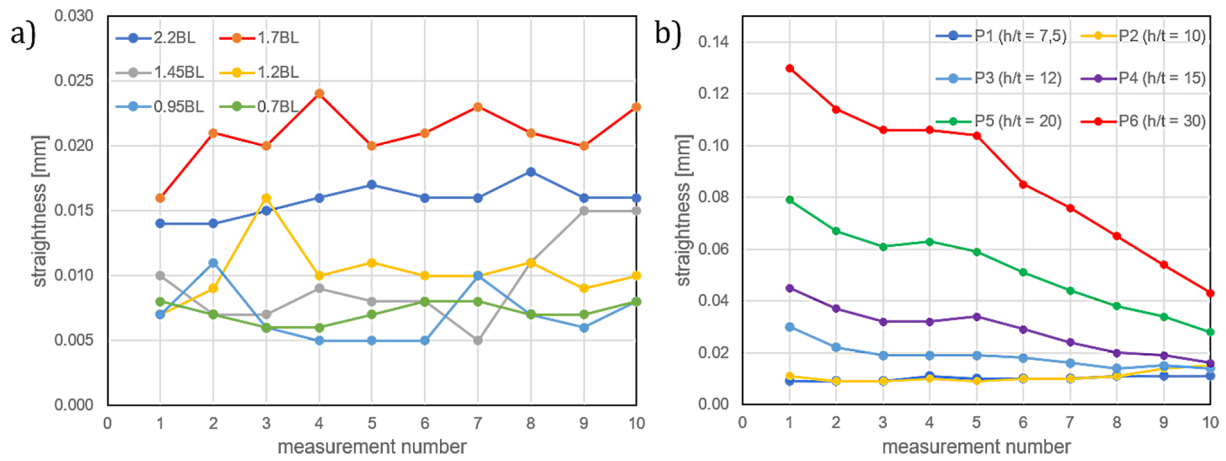
309

Fig. 16. Comparison of straightness of: (a) blank and (b) research samples
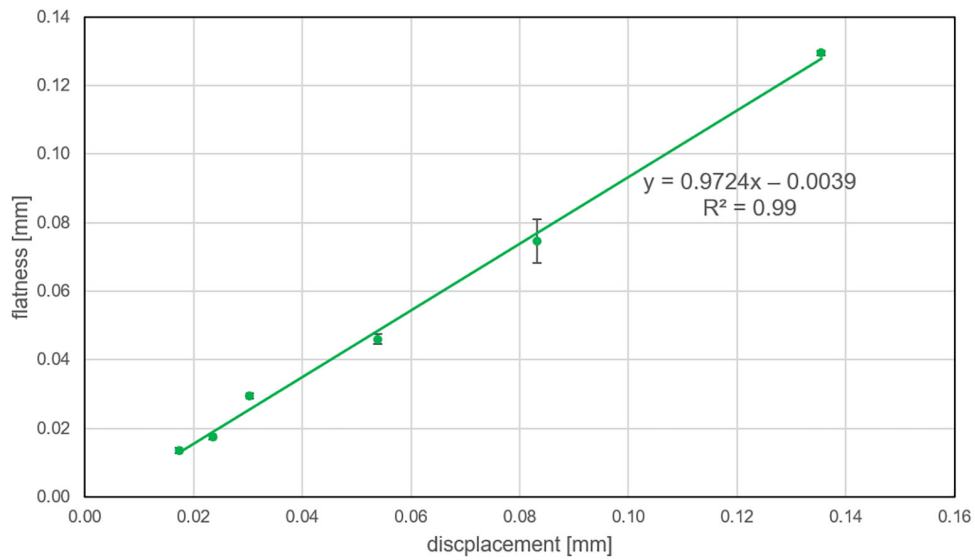

Fig. 17. Combination of deformation during machining with the flatness of a thin-walled element
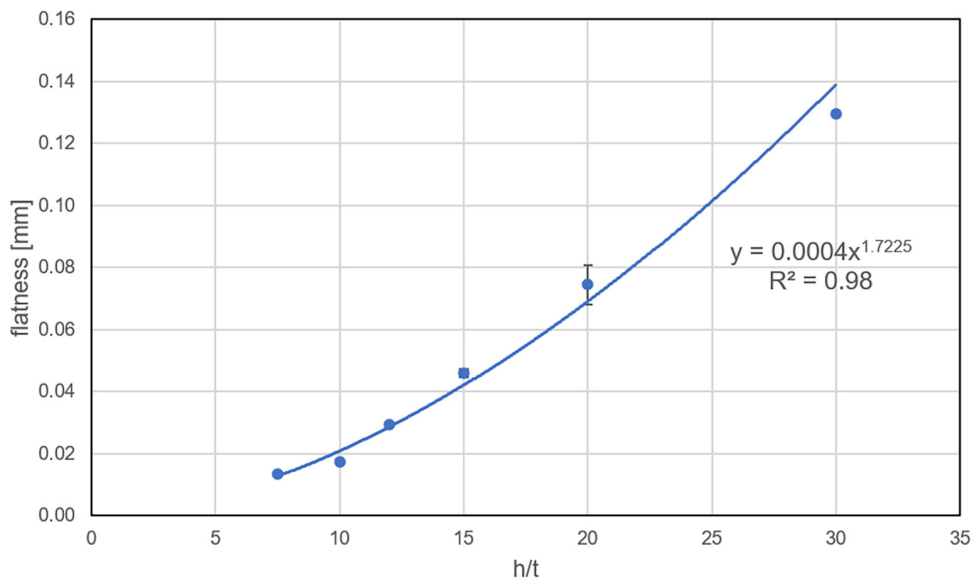

Fig. 18. Comparison of the h/t ratio with the flatness of the thin-walled element

of height to thickness *h*/*t*. In order to reduce the weight of the workpiece, it must be taken into account the difficulty or impossibility of obtaining the assumed geometrical accuracy. Figure 19 shows the reaction of a thin-walled element in the form of a straight-form wall also made of PA9 aluminum alloy under similar cutting conditions [12]. Only a deformation caused by milling of 85 µm can be seen in it, i.e. similar to figure 10, the return of the wall to its initial position is sudden and without deformation. This proves the lack of thermal deformation due to the shape of the sample. A different situation can be seen in the presented studies. This gives the first important conclusion that the shape of the wall is critical to the accuracy after machining. This was also confirmed by research [16] on a different scale.

The previously discussed section DE in figure 10 shows the time in which the wall returns to a stable state after milling. The result of this return, which in this case lasts 3.6 s is thermal deformation due to thermal expansion of the workpiece made of aluminum alloy. The thermal expansion coefficient of the EN AW-7075A alloy is 23.5 µm/m °C and the thermal conductivity is 134 W/mK. For comparison, grade 5 titanium alloy (Ti6Al4V) has a thermal expansion coefficient of 9 µm/m °C, respectively, and its thermal conductivity is 6.6 W/mK. On this basis, it can be concluded that the thermal conductivity of the material will affect the "cooling down" time of the wall, i.e. the length of the DE section. The tests carried out (not yet published) on the grade 5 titanium alloy during milling of identical thin-walled
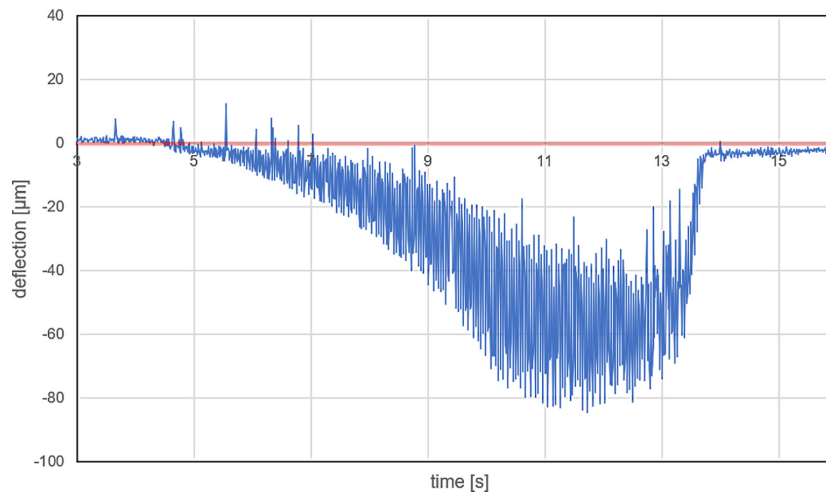

Fig. 19. An exemplary course of deformations during milling of a straight-form wall [12]
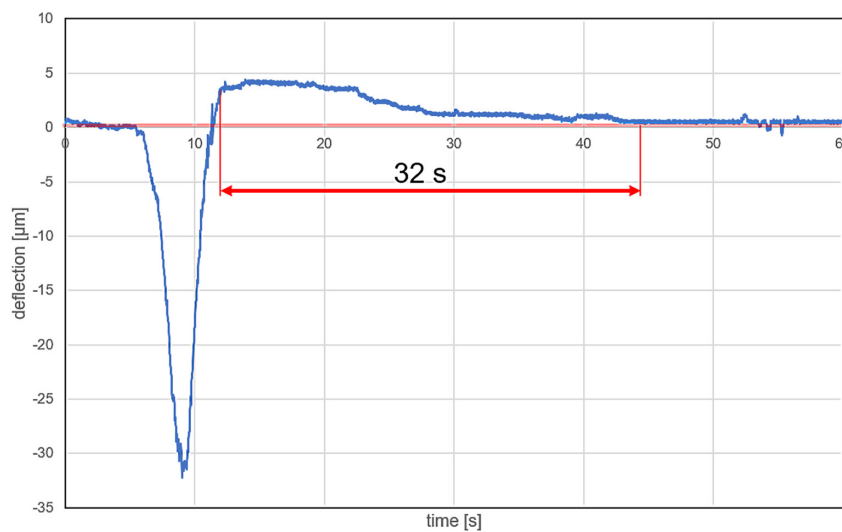

Fig. 20. An exemplary course of deformations during milling in one pass of a sample made of grade 5 titanium alloy (Ti6Al4V)

elements show an example of the deformation course in Figure 20. The wall reaction to milling and the reaction after milling are visible, similarly to the aluminum alloy, it should be noted that the recovery is much longer thin-walled element to a stable state, in this case it is about 32 s. In addition, during the machining of titanium alloys, permanent distortion did not always occur, as can be seen in the example. This may be due to the higher Young's modulus of titanium alloys.

The effect visible in the graph in Figure 20 shows how long it takes a thin-walled element made of titanium alloy to return to the ambient temperature and a stable state. Both titanium and aluminum alloys are machined in most cases with a cooling-lubricating liquid, which should significantly reduce this time [26], but it was not used in the test conditions. Current trends are focused on machining using the MQL method or excluding the use of cooling and lubricating liquids [27]. The discussed effect may affect the machining accuracy in the case of multi-row milling with high feeds, where the workpiece does not have time to cool down earlier and its thermal deformation will not remove the assumed layer of material in the next pass. It can be seen such a case in the Figure 21. The thin-walled element after the first pass did not manage to return to a stable state before the second pass, the deformed workpiece was processed through the second pass. The temperature during finishing machining was in the

range of 60–100 ºC, on the basis of this type of measurement it is not possible to determine the temperature at the point of contact of the endmill with the workpiece, but it gives a certain idea of the nature of the deformation itself. In the next stages, these results will be used for calculations in the FEM environment in order to create a deflection model of thin-walled elements. Research shows a significant impact of the shape of a thin-walled element on deformations after machining - hence, it would be a great saving of time and money to create in the FEM environment the possibility of testing various geometric shapes in this respect. As an assessment of dimensional and geometrical accuracy after machining, among others, straightness and flatness of the surface after milling were selected. The results show how much the machining strategy has an impact on the accuracy. Blank samples confirm the effectiveness of machining thin-walled elements by using small depths of cut and alternately milling both sides of the wall [8]. Finish milling was carried out at the full depth of cut ap = 15 mm, such a strategy allows for the study of deformations and temperature during machining. In addition, it provides the shortest possible cutting time - hence attempts are made to obtain similar machining accuracy as other strategies.

According to [3], when machining thin-walled workpieces, we do not obtain machining of the assumed cut layer due to deflection of the
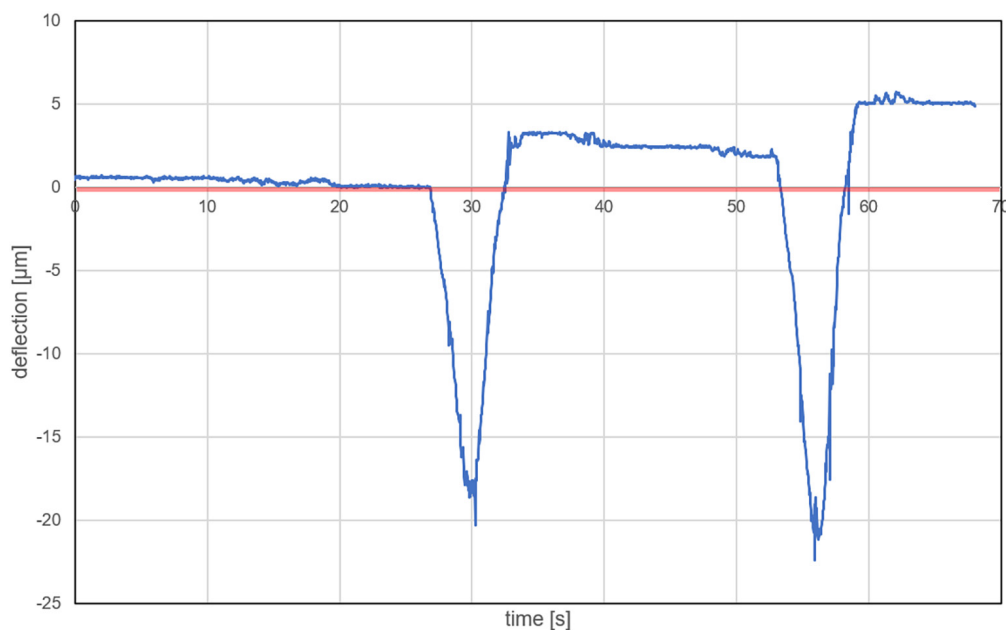

Fig. 21. An exemplary course of deformations during milling in two passes of a sample made of grade 5 titanium alloy (Ti6Al4V)

Table 4. Comparison of the distortion of a thin-walled element with the deformation during milling

Sample	h/t	Distortion I [mm]	Distortion II [mm]	Deformation I [mm]	Deformation II [mm]	%	
						Def. 1	Def. 2
P2S1	10	0.0035	0.0023	0.01880	0.02150	18.6	10.7
P2S2		0.0004	0.0033	0.02060	0.02550	1.9	12.9
P3S1	12	0.0088	0.0016	0.02640	0.03600	33.3	4.4
P3S2		0.0010	0.0008	0.01690	0.02390	5.9	3.3
P4S2	15	0.0050	0.0017	0.03640	0.04840	13.7	3.5
P4S3		0.0008	0.0034	0.04120	0.06020	1.9	5.6
P5S1	20	0.0040	0.0005	0.06270	0.08880	6.4	0.6
P5S2		0.0050	0.0014	0.04610	0.07310	10.8	1.9
P6S2	30	0.0054	0.0084	0.07700	0.14200	7.0	5.9
P6S3		0.0057	0.0052	0.07270	0.13270	7.8	3.9

wall from the cutter. This can be seen in figure 13 where at the top of the tested walls the thickness value differs significantly from the nominal one. The aforementioned deformation causes not only the non-removal of part of the material on the side where the part is milled, but deformation of the entire wall, causing its total deflection. The result is that the unmachined side does not return to its original position. Coordinate testing did not detect this deflection; it was directed more at the accuracy of the milled side itself. Table 4 shows the comparison of distortion of a thin-walled element (the aforementioned DE section) to deformation during milling. The last two columns show the percentage of distortion versus deformation. The percentages in both cases take values in the range of 0.6% to 33.3%, P1 specimens with an h/t ratio of 7.5 have been omitted due to anomalously in the deformation courses.

CONCLUSIONS

The machining of thin-walled workpieces poses many difficulties and requires a different approach. Very important is the shape and material of the workpiece, as shown in the study. The research carried out on straight-form walls may give unsatisfactory results if the knowledge from this research is transferred to real objects with more complex shapes. Based on the above research, several main conclusions can be drawn. Comparing the "blank" and test samples, the effect of the choice of milling strategy on post-machining accuracy in favor of the former is evident. Analyzing the deformation courses during milling, it can be seen on them the deformation caused by milling

and the reaction of the workpiece in the form of elastic and thermal deformation. In addition, there is a permanent distortion. The data obtained from measuring the temperature of the thin-walled component during machining will serve as data for numerical simulations of thermal deformation that will be implemented in further research. The shape of the thin-walled workpiece and the choice of material influence the occurrence of permanent deformation after machining. The geometric and dimensional accuracy after machining changes nonlinearly as the *h/t* ratio increases. When machining thin-walled workpieces made of materials with low thermal conductivity such as titanium alloys, the risk of accumulating thermal deformation must be kept in mind.

REFERENCES

1. Bao Y., Wang B., He Z., Kang R., Guo J. Recent progress in flexible supporting technology for aerospace thin-walled parts: A review. Chinese Journal of Aeronautics 2021; 1–17.

2. Qu S., Zhao J., Wang T. Experimental study and machining parameter optimization in milling thin-walled plates based on NSGA-II. Int J Adv Manuf Technol 2017; 89(5–8): 2399–409.

3. Izamshah R.A. R., Mo J., Ding SL. Finite Element Analysis of Machining Thin-Wall Parts. KEM 2010; 458: 283–8.

4. Wu Q., Li L., Zhang YD. Simulations and Experiments on Vibration Control of Aerospace Thin-Walled Parts via Preload. Shock and Vibration 2017; 2017: 1–7.

5. Kolluru K., Axinte D., Becker A. A solution for minimising vibrations in milling of thin walled casings by applying dampers to workpiece surface. CIRP Annals 2013; 62(1): 415–8.

6. Zhu W., Zhuang J., Guo B., Teng W., Wu F. An optimized convolutional neural network for chatter detection in the milling of thin-walled parts. Int J Adv Manuf Technol 2020; 106(9–10): 3881–95.

7. Zawada-Michałowska M. High-Performance Milling Techniques of Thin-Walled Elements. Adv Sci Technol Res J 2022; 16(3): 98–110.

8. Kuczmaszewski J., Zaleski K., Matuszak J., Mądry J. Testing Geometric Precision and Surface Roughness of Titanium Alloy Thin-Walled Elements Processed with Milling. Advances in Manufacturing II 2019; 5: 95–106.

9. Rubeo M.A., Schmitz T.L. Global stability predictions for flexible workpiece milling using time domain simulation. Journal of Manufacturing Systems 2016; 40: 8–14.

10. Shi J., Song Q., Liu Z., Ai X. A novel stability prediction approach for thin-walled component milling considering material removing process. Chinese Journal of Aeronautics 2017; 30(5): 1789–98.

11. Soori M., Asmael M. Deflection Error Prediction and Minimization in 5-Axis Milling Operations of Thin-Walled Impeller Blades. Mechanical Engineering 2021; 1–21.

12. Czyżycki J., Twardowski P., Znojkiewicz N. Analysis of the Displacement of Thin-Walled Workpiece Using a High-Speed Camera during Peripheral Milling of Aluminum Alloys. Materials 2021; 14(16): 4771.

13. Czyżycki J., Twardowski P. Evaluation of Deflection of Thin-Walled Profile During Milling of Hardened Steel. Industrial Measurements in Machining 2020; 22–32.

14. Bałon P., Rejman E., Świątoniowski A., Kiełbasa B., Smusz R., Szostak J., Szostak., Cieślik J., Kowalski Ł. Thin-walled Integral Constructions in Aircraft Industry. Procedia Manufacturing 2020; 47: 498–504.

15. Hussain A., Lazoglu I. Distortion in milling of structural parts. CIRP Annals 2019; 68(1): 105–8.

16. Zawada-Michałowska M., Kuczmaszewski J., Pieśko P. Effect of the Geometry of Thin-Walled Aluminium Alloy Elements on Their Deformations after Milling. Materials 2022; 15(24): 9049.

17. Zhu P., Liu Z., Ren X., Cai Y. Machining Distortion for Thin-Walled Superalloy GH4169 Caused by Residual Stress and Manufacturing Sequences. Metals 2022; 12(9): 1460.

18. Jiang X., Wang Y., Ding Z., Li H. An approach to predict the distortion of thin-walled parts affected by residual stress during the milling process. Int J Adv Manuf Technol 2017; 93(9–12): 4203–16.

19. Jiang X., Li B., Yang J., Zuo XY. Effects of tool diameters on the residual stress and distortion induced by milling of thin-walled part. Int J Adv Manuf Technol 2013; 68(1–4): 175–86.

20. Gang L. Study on deformation of titanium thin-walled part in milling process. Journal of Materials Processing Technology 2009; 209(6): 2788–93.

21. Chen W., Xue J., Tang D., Chen H., Qu S. Deformation prediction and error compensation in multilayer milling processes for thin-walled parts. International Journal of Machine Tools and Manufacture 2009; 49(11): 859–64.

22. Kuczmaszewski J., Łogin W., Pieśko P., Zagórski I. State of Residual Stresses After the Process of Milling Selected Aluminium Alloys. Adv Sci Technol Res J 2018; 12(1): 63–73.

23. Wang T., Zha J., Jia Q., Chen Y. Application of low-melting alloy in the fixture for machining aeronautical thin-walled component. Int J Adv Manuf Technol 2016; 87(9–12): 2797–807.

24. Scippa A., Grossi N., Campatelli G. FEM based Cutting Velocity Selection for Thin Walled Part Machining. Procedia CIRP 2014; 14: 287–92.

25. Meshreki M. Dynamics of Thin-Walled Aerospace Structures for Fixture Design in Multi-axis Milling. Journal of Manufacturing Science and Engineering 2008; 130(3): 031011.

26. Su Y., He N., Li L., Li XL. An experimental investigation of effects of cooling/lubrication conditions on tool wear in high-speed end milling of Ti-6Al-4V. Wear 2006; 261(7–8): 760–6.

27. Singh G., Aggarwal V., Singh S. Critical review on ecological, economical and technological aspects of minimum quantity lubrication towards sustainable machining. Journal of Cleaner Production 2020; 271: 122185..